

# PHYSICO-CHEMICAL AND NONLINEAR-OPTICAL PROPERTIES OF $V_2O_5$ QUANTUM DOTS AND QUANTUM RODS IN PVA

A.S. KUTSENKO, S.M. MALOLETOV, S.YA. KUCHMII,  
V.R. LYAKHOVETSKY<sup>1</sup>, V.I. VOLKOV<sup>1</sup>, A.A. BORSHCH<sup>1</sup>, P.M. LYTVYN<sup>2</sup>

© 2004

**Pisarzhevsky Institute of Physical Chemistry, Nat. Acad. Sci. of Ukraine**  
(31, Nauky Prosp., Kyiv 03039, Ukraine),

<sup>1</sup>**Institute of Physics, Nat. Acad. Sci. of Ukraine**  
(46, Nauky Prosp., Kyiv 03650, Ukraine; e-mail: volkov@iop.kiev.ua),

<sup>2</sup>**Institute of Semiconductor Physics, Nat. Acad. Sci. of Ukraine**  
(45, Nauky Prosp., Kyiv 03028, Ukraine)

$V_2O_5$ /polyvinyl alcohol (PVA) nanocomposite and its thin films [(1–10)  $\mu\text{m}$ ] were synthesized and studied by means of electron (UV, visible, near IR spectral range) and EPR spectroscopies. The presence of quantum dots and quantum tapes of  $V_2O_5$  in the composite has been approved by means of X-ray diffraction and Atomic Force Microscope (AFM) studies. The nonlinear refraction of the samples has been studied in the schemes of degenerate four-wave mixing and Z-scan. The sign and value of the nonlinear refractive index coefficient  $n_2$  have been determined. Possible mechanisms of the nonlinear refraction are discussed. It has been shown that the composite polymer material containing nanoparticles of  $V_2O_5$  and the low glass transition temperature polymer matrix exhibit a high third-order optical nonlinearity [ $\chi^{(3)}(\omega; \omega, -\omega, \omega) = 2.4 \cdot 10^{-15} \text{ m}^2/\text{V}^2$ ] and can be used as a medium for the holographic recording by a single laser pulse with the 10-ns duration.

composite materials with nanocrystals of  $\text{CdS}_x\text{Se}_{1-x}$  [2] and PbS [3]. At the same time, chalcogenide nanocrystals turned out to be unstable. Due to the oxidation in the glass matrix, chalcogenide nanoparticles change their color during some years, meantime a heating at 300° takes only several hours for the process to take place [4], the activation energy being equal to (111±6) kJ/mol. Such a phenomenon in glass doped by chalcogenides may sufficiently restrict using the porous glass matrix for such materials. On the other hand, the illumination of chalcogenide nanoparticles by intense light causes photocorrosion or photoetching, which can be used for producing monodisperse nanoparticles of ZnS [5], CdS [6] and PbS [7].

## Introduction

Searching for new effective materials for optoelectronics, microelectronics, and molecular electronics is constantly carried out by scientists all over the world. This promises to improve the performance of electronic devices. Composite materials based on semiconductor nanocrystals and organic polymers exhibit unique properties and are perspective materials for applications in optoelectronics and nonlinear optics (NLO). The main demands, which are made to the materials, are optical homogeneity, transparency, optical stability, and high NLO sensitivity. To obtain the optical homogeneity and the absence of scattering in the materials, the size of nanoparticles has to be less than a quarter of a light wavelength. The polymer matrix of a composite should be transparent in a given spectral range. The third-order optical nonlinearity was mainly studied in composite materials containing chalcogenides  $A_2B_6$  [1]. The highest NLO sensitivity has been observed in

The problem of photostability of inorganic nanocrystals is connected with the presence of oxygen, whose content in the air is 21% and is, e.g., 6.35  $\text{cm}^3/\text{l}$  in water [8]. In the contemporary scientific literature, the implementation of dendrimers and dendrons is recommended to prevent the photocorrosion of chalcogenide nanocrystals [9, 10] and metals [11–13]. Dendrons and dendrimers are organic ligands with branchy structure covalently attached to nanoparticles. Such a structure of the organic ligand prevents oxygen to reach inorganic nanocrystals. The sufficient progress was achieved while using this technique. Thus, for example, it was shown in [10] that the increase of the ligand branchy structure makes it possible to increase the photochemical stability of CdSe nanocrystals by a factor of 10. Another way to cope with the problem of nanocrystal photostability is to use semiconductor-oxides stable against photocorrosion. The third-order optical nonlinearity of epitaxial layers of 30–80 nm in thickness of a set of oxides (among others,  $V_2O_5$ ,  $\text{Fe}_2\text{O}_3$ ,  $\text{CuO}$ ,  $\text{Co}_3\text{O}_4$ ,  $\text{Mn}_3\text{O}_4$ ,  $\text{Cr}_2\text{O}_3$ , and  $\text{NiO}$ ) has been studied

in [14]. The first three oxides were shown to have the highest NLO sensitivity under excitation by 7-ns laser pulses at  $\lambda=532$  nm. The value of the third-order optical susceptibility of  $V_2O_5$  was six times higher than that of  $Fe_2O_3$  and  $CuO$  and comparable with the susceptibility of nanocrystals of  $CdS_xSe_{1-x}$  [2] and  $PbS$  [3].

We have chosen vanadium oxide as an object for our studies. We have supposed that the composites containing nanoparticles of vanadium oxide should have high NLO sensitivity because epitaxial layers with  $V_2O_5$  have shown the high third-order NLO response. As a polymer matrix, we have chosen polyvinyl alcohol (PVA). The polymer is optically stable, because the photochemical reactions do not run in it under excitation of the polymer by a powerful light with  $\lambda=532$  nm [3].

## 1. Experiment

X-ray structure analysis was performed using a DRON-4.07 diffractometer ( $CuK_\alpha$ -radiation,  $\lambda = 1.54178$  Å).

The thickness of our samples has been measured by means of a Linnik micro interferometer MII-4 using the difference of the positions of zero interference fringes at light reflectance from the film surface and the substrate surface for the calculations.

The electronic absorption spectra were obtained by means of a spectrophotometer SF-20M.

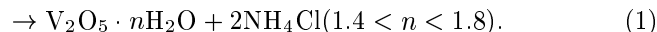
The EPR spectroscopy measurements have been carried out by using an EPR spectrograph Varian E-9.

The sample surface morphology was studied by means of an AFM-digital instrument Nano Scope 111a.

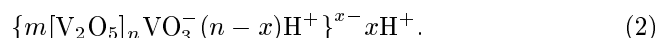
The nonlinear refraction in the samples was studied by dynamic holographic grating recording in the scheme of degenerate four-wave mixing. A one-mode frequency-doubled YAG:Nd<sup>3+</sup> laser ( $\tau = 10$  ns,  $\lambda = 532$  nm, TEM<sub>00</sub>) was used as the light source. Read out of the dynamic gratings was carried out using a cw He-Ne laser. The interference field of the two interacting coherent light beams from the pulsed laser induced in the sample a dynamic grating based on the refractive index modulation, at which the self-diffraction of the recording beams was observed. The sign of the refractive index nonlinear change was determined using data obtained by Z-scan technique.

### *Synthesis of $V_2O_5$ Nanoparticles and Sample Fabrication*

We used the Bilts technique [15] for the synthesis of  $V_2O_5$  nanoparticles:



In reaction (1), it is shown that a  $V_2O_5$  sol contains some amount of water bound to it. Solubility of  $V_2O_5$  is high enough so that soles are getting deteriorated very rapidly due to both relatively big growing particles and their deposition on the vessel bottom. The soles synthesized in such a way contain the admixture of  $Cl^-$  and  $NH_4^+$  ions. We used the dialysis to remove the admixture. Mainly due to this operation, it is possible to obtain a monodisperse sol which does not contain electrolytes and is not getting deteriorated [16]. The following scheme of the  $V_2O_5$  micelle formation was suggested in [16]:



It is seen from the scheme that  $V_2O_5$  sol nanoparticles have negative sign (-). A solution of PVA in distilled water was added after dialysis.

Thin film samples have been obtained by means of spreading the solution onto the 30×30 mm glass plates. The PVA concentration in the solution was chosen in such a way that the concentration of  $V_2O_5$  in the film would be: 20, 40, 60, 80 and 100%. The thickness of the obtained layers was from 1 to 10 μm. The film thickness was varied in order to determine the optimal absorption of the light with  $\lambda = 532$  nm, at which the method for measuring the third-order NLO susceptibility, which we used, was the most sensitive.

### *Composite Material Structure Characterization*

Fig. 1 shows the dimensions and the layered structure of  $V_2O_5$  nano-sized tapes taken from [17]. The  $V_2O_5$  nano-tape formation was investigated in detail in [18–20] using electron microscopy. Fig.2 presents the photographs of  $V_2O_5$  sol shaded in by gold taken just after fabrication, five days later, and after three-year storing [19]. One can clearly see that the structure of  $V_2O_5$  sol is changed with time. The analysis of the results obtained by different authors made it possible to clarify the process of  $V_2O_5$  nano-tape formation. At the beginning of the synthesis, shapeless amorphous particles are appeared. Then needle-like particles are formed from them. While the sole is getting deteriorated, the needles are combined into tapes, their length being gradually increased. With time, the linkage of tapes forms a dense net [18]. The tapes in the net are long and almost have no branching. So, the process of polymerization with the formation of an inorganic polymer proceeds in such a way.

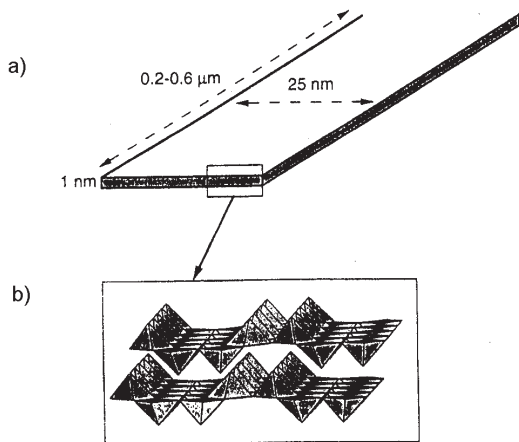


Fig. 1. Dimensions (a) and structure (b) of a  $V_2O_5$  nanostripe

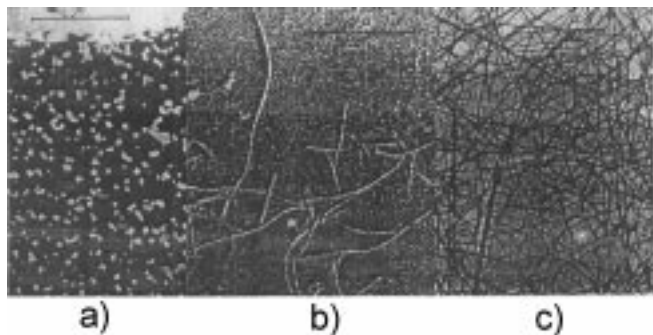


Fig. 2. Electron microscope pictures of the  $V_2O_5$  sol shaded by gold: a — just after synthesis, b — five days later, c —  $V_2O_5$  sol after the lapse of three years [18]

It is known that adding the small amount of an electrolyte to the sol sufficiently increases the speed of the tape formation. On the other hand, the growth of the tapes does not take place in a gel where there is no collisions of colloidal particles. It was shown in [19] that the mechanisms of particle growth in  $V_2O_5$  sol may be different depending on the electrolyte content. At a low electrolyte concentration in sol, the crystallization prevails and proceeds due to both dissolving the smaller particles and decreasing the amount of actually dissolved  $V_2O_5$ . Meanwhile at higher concentrations of electrolytes, the coagulation of oriented particles dominates. That is, long tapes can be grown only in the case where particles can aggregate only at two points, the ends of a tape.

In our studies, the colloids for samples with the  $V_2O_5$  concentrations of 20, 40, and 60% were stabilized by PVA just after the fabrication. Then the samples were taken from the solutions. The stabilization of the colloids

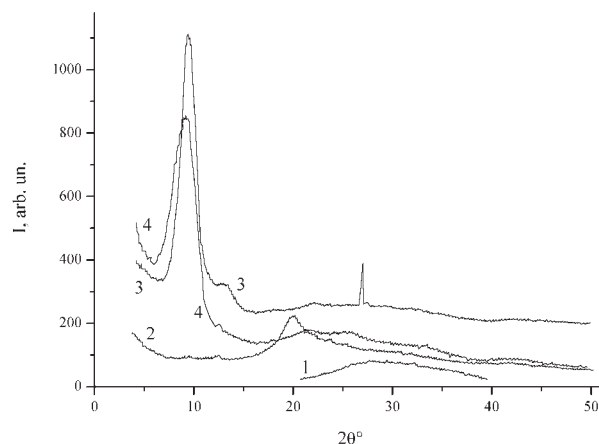


Fig. 3. X-ray diffraction pattern of xerogel and  $V_2O_5$  composite: 1 — glass substrate, 2 — PVA film, 3 —  $V_2O_5$  xerogel film, 4 — composite material (80% of  $V_2O_5$  and 20% of PVA)

was necessary to prevent the crystal structure formation. In contrast to that, in the case of a  $V_2O_5$  concentration of 80%, the colloid was kept up for five days and then stabilized by PVA. After that, the dialysis was conducted to remove the electrolytes from the solution. The purpose of this procedure, i.e. stabilization and removing the electrolytes, was to stimulate the formation of the  $V_2O_5$  crystalline tape structure and to provide the long-lived stability of the colloid. In fact, the obtained colloid stability is unchanged for more than a year.

The obtained X-ray diffraction pattern is shown in Fig. 3. Curve 1 in the graph corresponds to the amorphous glass plate structure. Curve 2 recorded for a PVA film of 0.5 mm in thickness has a peak at  $2\theta \approx 20^\circ$  typical of such a polymer [21]. Curve 3 presents the data obtained for a  $V_2O_5$  xerogel film on the glass substrate. The curve has two reflexes from surfaces (001) at  $2\theta \approx 10^\circ$  and (002) at  $2\theta \approx 27^\circ$  which are typical for the crystalline tape structure of  $V_2O_5$  xerogel synthesized by the Bilts technique. Curve 4 in Fig. 3 presents the X-ray diffraction pattern for the composite material containing 80% of  $V_2O_5$  xerogel and 20% of PVA. The curve shows the contribution from the amorphous substrate and the polymer matrix as well as the more pronounced peak from (001) surface of the  $V_2O_5$  xerogel crystalline structure. Comparing curves 3 and 4 in Fig. 3, we can conclude that the absence of a reflex from (002) surface and some broadening in reflex from (001) surface of  $V_2O_5$  xerogel in the composite material relative to pure  $V_2O_5$  xerogel are the evidence for the poor crystalline quality of the xerogel in PVA.

Meantime some shift in the position of (001) reflex for the xerogel in PVA towards smaller angles could be attributed to the intercalation of PVA molecules between the crystalline surfaces of the xerogel, as it takes place in the case of water-soluble polyaniline [22].

Using formula

$$d = \lambda / (2 \cdot \sin\theta), \quad (3)$$

where  $\lambda = 1.5405 \text{ \AA}$  under  $\text{CuK}\alpha$  irradiation, we have estimated the intersurface distance for  $\text{V}_2\text{O}_5$  xerogel. It turned out that  $d = 9.6 \text{ \AA}$  for pure  $\text{V}_2\text{O}_5$  xerogel and  $d = 10.2 \text{ \AA}$  for  $\text{V}_2\text{O}_5$  in PVA, that is  $\Delta d = 0.6 \text{ \AA}$ . Such an insufficient intercalation in PVA can be attributed to the small concentration of the polymer (only 20%) and to the fact that the molecules of the linear polymer PVA are mainly clewed up in water, so that they have no opportunity to contact with a linear crystalline tape of  $\text{V}_2\text{O}_5$  over a sufficiently long length.

None crystalline structure has been registered in the diffraction patterns taken for the samples with the  $\text{V}_2\text{O}_5$  concentrations of 20, 40, and 60%. In this case, the sol has been stabilized by PVA just after synthesis and has not been kept for a long time before that. Thus, the composite material with 80% of  $\text{V}_2\text{O}_5$  was of a crystalline structure and those with 20, 40, and 60% concentrations were amorphous as a result of different techniques of synthesis.

### Sample Surface Morphology

We have studied the surface morphology of  $\text{V}_2\text{O}_5$  xerogel films and the composite material containing 80% of  $\text{V}_2\text{O}_5$  and 20% of PVA. Thermal stability of the nanotapes in the samples with  $\text{V}_2\text{O}_5$  xerogel has been verified by means of the thermal annealing at  $240 \text{ }^\circ\text{C}$  and  $300 \text{ }^\circ\text{C}$  during 30 min. It is known [23] that PVA has the low glass transition temperature  $T_g = 85 \text{ }^\circ\text{C}$ , so that the samples of composite materials were not annealed.

To obtain the well-defined images of  $\text{V}_2\text{O}_5$  xerogel tapes with a microscope, it was necessary to have samples with oriented nanotapes. Nanotapes of  $\text{V}_2\text{O}_5$  are known to be oriented in water sol by means of a magnetic field or polarized light. We decided to use a simpler method, the "method of orientation in a flow" [24], and used it, for the first time, for the orientation of  $\text{V}_2\text{O}_5$  xerogel tapes.

The obtained data on the surface morphology of the above-mentioned films are shown in Fig. 4. The surface relief of the films under study is presented by gray hues: white color corresponds to the maximum of the relief, dark one — to the minimum. Fig. 4, a shows the  $\text{V}_2\text{O}_5$

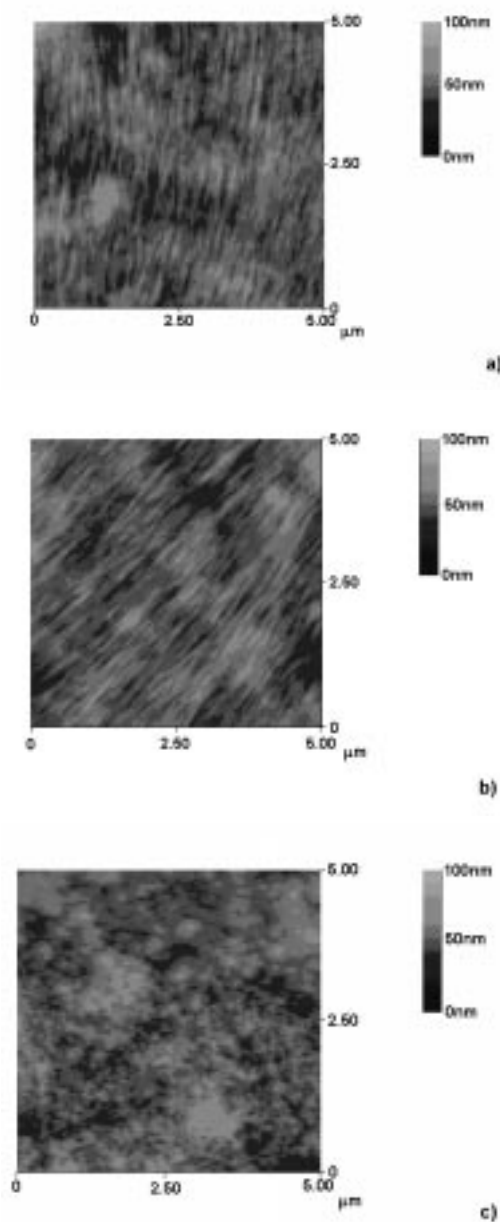


Fig. 4. Film surface morphology: a —  $\text{V}_2\text{O}_5$  xerogel, b —  $\text{V}_2\text{O}_5$  xerogel after 30 min annealing at  $240 \text{ }^\circ\text{C}$ , c — composite material (80% of  $\text{V}_2\text{O}_5$  and 20% of PVA)

xerogel film surface morphology before annealing. It is seen that, before the annealing, the surface consists of oriented fibers with a width of 100 nm and a length of about 1500 nm. The averaging roughness of the surface fragment under study was 5.48 nm. The result of our experiments shows that the method of orientation in a

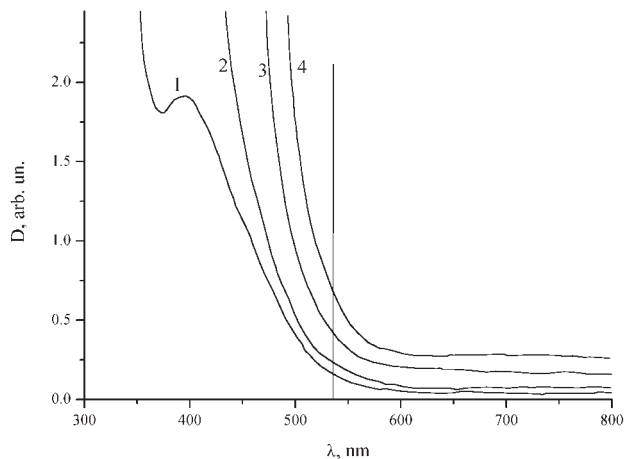


Fig. 5. Absorption spectra of the composite material (80% of  $V_2O_5$  and 20% of PVA) films obtained from the solutions: 1 – 0.20 ml, 2 – 0.25, 3 – 0.3, 4 – 0.4, respectively

flow is efficient. As seen from Fig. 4, *b*, the annealing of the sample at 240 °C did not change the morphology sufficiently: the width of the fibres on the surface and their length were not changed. The average roughness of the surface was not changed as well – its value was 5.45 nm again. The average width of the fibres turned out to be larger than that of a single tape in Fig. 1 because a fibre possibly consists of several nanotapes. Our experiments show that the fibres are almost completely disoriented or even destroyed after the annealing at 300 °C.

The morphology of the composite material with 80% of  $V_2O_5$  and 20% of PVA is shown in Fig. 4, *c*. Two types of morphology can be seen on the surface: granular (roughness of 3.5 nm) and fern-shaped (roughness of 4.47 nm). In the case of the granular morphology, the size of the biggest granules is 250–300 nm, and they are tightly packed and have sharp borders. Sizes of separate elements in the fern-shaped surface area are 400 nm in length and 150 nm in width. From the experiment results, it is seen that the surface morphologies of the xerogel and composite material are principally different. It is clear that there is a connection between the surface morphology and the composition of the films and their properties.

### Electron and EPR Spectroscopy

The absorption spectra of the composite material (80%  $V_2O_5$  and 20% PVA) are shown in Fig. 5. Samples of the material were made from the following solutions: 1 – 0.15 ml; 2 – 0.25; 3 – 0.3; 4 – 0.4. The vertical line

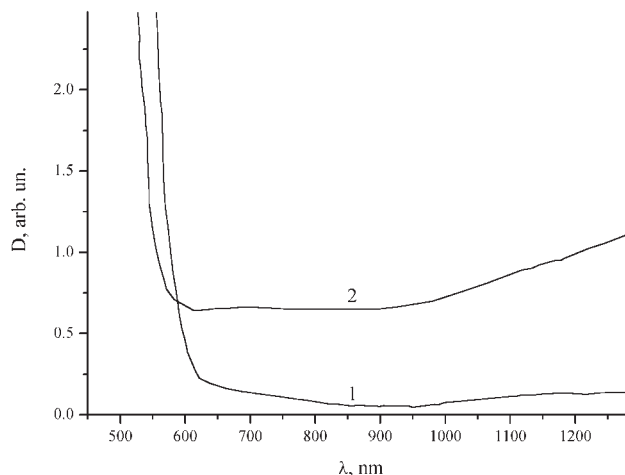


Fig. 6. Absorption spectra of the  $V_2O_5$  zol stabilized by PVA. 1 – ten days after the synthesis; 2 – eleven months after the synthesis

in Fig. 5 shows the spectral position of the light wavelength  $\lambda=532$  nm which was used for the NLO studies. The absorption spectra of the samples with different  $V_2O_5$  concentrations are similar to that shown in Fig. 5. Values of the forbidden gaps of colloidal  $V_2O_5$  which we determined by using absorption spectra are similar to that for bulk  $V_2O_5$ ,  $E_g \sim 2.25$  eV [25]. This is a direct manifestation of the absence of the quantum dimensional effect in our samples. For our studies, the quantum dimensional effect was not necessary. The effect has to cause the absorption spectra to shift towards the short-wave spectral range resulting in the absorption and NLO response decrease at  $\lambda = 532$  nm.

In [26], this was demonstrated for the xerogel electron transitions at  $\lambda = 192$ ; 268; and 381 nm in the region of the fundamental absorption. A decrease of the thickness of the samples with 80% of  $V_2O_5$  leads to the appearance of the absorption band (Fig. 5, curve 1) corresponding to the electron transition with  $\lambda=381$  nm [26].

The absorption spectra of the  $V_2O_5$  sol stabilized by PVA are shown in Fig. 6 [10 days keeping under normal conditions after the synthesis (curve 1) and 11 months after the synthesis (curve 2)]. In [26], three very weak absorption bands of forbidden  $d-d$  transitions in the visible spectral range 600 – 800 nm and two absorption bands of intervalent V(V)–O–V(IV) transitions with maxima at 1408 and 1515 nm have been found for the  $V_2O_5$  xerogel. In the spectra shown in Fig. 5 taken for  $V_2O_5$  composite material and in Fig. 6 for  $V_2O_5$  sol stabilized by PVA, the  $d-d$  transitions have not been observed in the spectral range from 600 to 800 nm. In the near IR, however, we have observed a pronounced

absorption band (Fig.6, curve 1) in the  $V_2O_5$  sol ten days after synthesis. The band is slowly increased from 900 to 1300 nm, which is a direct evidence for the intervalent V(V)—O—V(IV) transitions. The intensity of the band was considerably increased after keeping the  $V_2O_5$  colloid stabilized by PVA up for 11 months. Such a wide band in the near IR is considered to be caused by the absorption of a small-radius polaron [27], which is a result of the V(V) PVA reduction.

The data obtained by EPR give also the evidence for the vanadium (V) to vanadium (IV) reduction. The EPR spectra for the  $V_2O_5$ /PVA composite material as well as for the vanadium oxide (IV) powder are shown in Fig. 7. It is seen that, both for room temperature and the frozen state, there are wide anisotropy reflexes with a low superfine structure due to the interaction between a non-paired electron and a magnetic vanadium nucleus (spin 7/2). The parameters of the reflexes are similar to that of vanadium (IV). It is interesting to note that, in the range of the  $g$ -factor of the free electron signal, one can observe the low-intensity five-component signal A with the HFS constant near 6 G (see the inset in Fig. 7) which can be attributed to an organic radical formed from PVA molecules and stabilized into a solid matrix.

### NLO Properties

As was mentioned above, the NLO properties of thin films of some oxides have already been studied [14]. Meantime, the NLO properties of the composite materials containing nanoparticles of oxides have not been studied yet. At the same time, such composite materials have been used for the information recording based on the thermal mechanism. It is known [28] that, in polymers with dyes under pulsed excitation, a local temperature can reach 200 °C. For instance in the case of  $Fe_3O_4$  nanoparticles in a composite [29], they are heated under irradiation. As a result, the polymer matrix near the particles softens so that  $Fe_3O_4$  particles are aligned in chains in the magnetic field. Such a state is then frozen when the matrix is cooled down. One- and two-dimensional gratings with diffraction efficiency up to 48% have been recorded in a  $V_2O_5$  composite material by ultrashort laser pulses with a pulse length of 0.5 ps [30]. Stationary diffraction gratings have been also recorded in our samples under some conditions. For instance, in our samples with thin semitransparent layers of 100%  $V_2O_5$  xerogel, we were able to record only stationary diffraction gratings. It is the promising property of the material for its using in systems for the information recording and storage by short laser pulses.

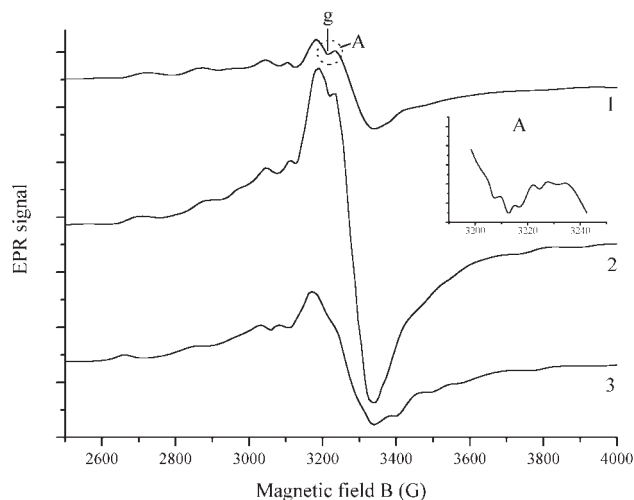


Fig. 7. EPR spectra of the  $V_2O_5$ /PVA composite (1, 2) and  $VO_2$  (3). 1 — at 20 °C; 2 — at 40 °C; 3 — at -196 °C

While studying the NLO properties, we could manage to record both stationary and dynamic gratings.

It should be noted that, in general, the transition from amorphous  $V_2O_5$  to its crystalline nanotapes resulted in both a higher photostability of our samples and their NLO sensitivity.

The nonlinear refraction in the samples was studied by the dynamic holographic grating recording in the scheme of degenerate two-wave mixing. A one-mode frequency-doubled YAG:Nd<sup>3+</sup> laser ( $\tau = 10$  ns,  $\lambda = 532$  nm, TEM<sub>00</sub>) was used as a light source. The nonlinear refractive index coefficient was estimated using the relation

$$n_2 = \lambda \cdot \sqrt{\eta} / (\pi \cdot \ell \cdot I_0), \quad (4)$$

where  $\ell$  is the sample thickness,  $I_0$  is the recording light intensity,  $\lambda$  is the light wavelength, and  $\eta$  is the diffraction efficiency.

For the sample with 80% of  $V_2O_5$ , we get  $n_2 = 1.39 \cdot 10^{-13}$  m<sup>2</sup>/W by using the following data:  $\ell = 3 \mu\text{m}$ ,  $I_0 = 3.5 \times 10^9$  W/m<sup>2</sup>,  $\lambda = 0.53 \mu\text{m}$ ,  $\eta = 7.43 \times 10^{-5}$ . The obtained value of  $n_2$  for our sample is three times higher than that for the composite material containing 19 mas.% 5 nm PbS particles in PVA [3] and is about 65% of  $n_2$  for bulk  $V_2O_5$  [14].

The third-order optical nonlinear susceptibility can be estimated from the expression

$$\chi^{(3)}(\omega) = 4/3 \varepsilon_0 c n_0^2 n_2, \quad (5)$$

where  $c$  is the light speed,  $\varepsilon_0$  is the absolute dielectric constant of vacuum,  $n_0$  is the refractive index which is

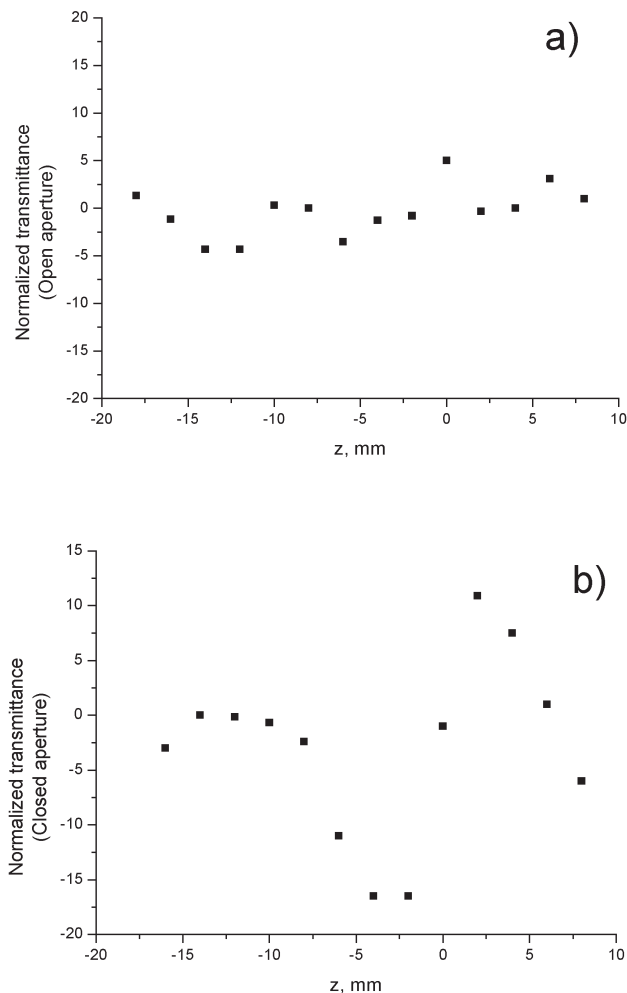


Fig. 8. Z-scan traces taken for the composite material (80% of  $V_2O_5$  and 20% of PVA)

in our case from 1.51 [23] to 2.37 [14] for the  $V_2O_5$  concentration from 0 to 100%.

For our sample containing 80% of  $V_2O_5$ , we may take  $n_0 = 2.2$  as an approximate estimation based upon the proportional dependence of  $n_0$  on the concentration. So, we may estimate the value of the third-order optical nonlinear susceptibility to be  $\chi^{(3)}(\omega) = 2.4 \times 10^{-15} \text{ m}^2/\text{V}^2$  for our sample.

Fig. 8 shows the Z-scan traces taken for the sample containing 40%  $V_2O_5$  and 60% PVA. The shape of the curve obtained with closed aperture corresponds to a positive nonlinear change of the refractive index ( $\Delta n > 0$ ). Taking into account the positive sign of the refractive index change and the fast time response (nanoseconds), we may conclude that the contribution

into the nonlinear refraction could be attributed to the nonlinear polarizability of bound (valent) electrons.

In our opinion, the main difference between oxide thin films and composite materials is the possibility to change the structure rigidity of a polymer matrix, which makes composite materials more universal from the point of view of practical applications in nonlinear optics and quantum electronics. So, the thermal stability of PVA is not high. Its glass transition temperature  $T_g = 85^\circ \text{C}$  [23]. This facilitates recording the stationary holograms. However, when the stationary recording have to be suppressed, it is necessary to use polymers with higher glass transition temperature for NLO composites. Therefore, the demand of matrix thermal stability has to be applied to NLO polymer materials in addition to the general demands mentioned above.

In conclusion, we have shown that composite polymer materials with a low glass transition temperature containing nanoparticles of transition metal oxides can be used as a register medium for pulsed recording (10 ns) of stationary holographic gratings. Meantime, in the case of high glass transition temperatures, it is possible to record dynamic holographic gratings. We have also shown the possibility to control the absorption spectra of  $V_2O_5$  nanotapes in the near IR spectral range. This is very promising for producing the fast and effective NLO materials for different pulsed laser sources in the near IR spectral range. It should also be noted that the composite materials containing nanoparticles of different nature have sufficient advantages in comparison with bulk materials due to the technological possibilities of a variation of material parameters and to the simplicity of the material synthesis.

1. *Beecroft L.L., Ober C.K.* // Chem.Mater. — 1997.— **9**. — P. 1302–1317.
2. *Jind R.K., Lind R.C.* // J. Opt. Soc. Amer.— 1983.— **73**, N 5.— P. 647–653.
3. *Kutsenko A.S., Maloletov S.M., Kuchmii S.Ya. et al.* // Theor. Exp. Chem. — 2002.— **38**, N 3. — P. 170–175.
4. *Nogami M., Kato A.* // J. Non-Cryst. Solids.— 1993.— **163**. — P. 242–248.
5. *Ohko Y., Setani N., Sakata N. et al.* // Chem. Lett.— 1999.— **7**.— P. 663–664.
6. *Matsumoto H., Sakata N., Mori H., Yaneyama H.* // J. Phys. Chem.— 1996.— **100**.— P. 13781–13785.
7. *Dijken A., Janssen A.H., Smitsmans M.H.P. et al.* // Chem. Mater.— 1998.— **10**.— P. 3513–3522.
8. *Geirisher H., Heller A.* // J. Phys. Chem.— 1991.— **95**, N 8.— P. 5261–5267.
9. *Aldana J., Wang Y.A., Peng X.* // J. Amer. Chem. Soc.— 2001.— **123**, N 36.— P. 8844–8850.

10. Wang Y.A., Li J.J., Chen H., Peng X. // *Ibid.*— 2002.— **124**, N 10.— P. 2293—2298.
11. Kim H.-K., Jeon Y.-M., Jeon W.S. et al. // *Chem. Commun.*— 2001. — N 7.— P. 667—668.
12. Zhao M., Crooks R.M. // *Chem. Mater.*— 1999.— N 11.— P. 3379—3385.
13. He S.-A., Valluzzir R., Yang Ke et al. // *Ibid.* — P. 3268—3274.
14. Ando M., Kadono K., Haruta M. et al. // *Nature.*— 1995.— **374**, N 6523.— P. 625—627.
15. *Handbook on Inorganic Synthesis* / Ed. by H. Brower.— Moscow: Mir, 1985 (in Russian).
16. Putilova I.N. *Handbook on Practical Studies on Colloid Chemistry.*— Moscow: Vyssh. Shkola, 1961 (in Russian).
17. Gabriel J.-C.P., Davidson P. // *Adv. Mater.*— 2000.— **12**, N 1.— P. 9—20.
18. Nemtsova V.V., Radushkevich L.V., Luk'yanovich V.M., Chmutov K.V. // *DAN SSSR.*— 1951.— **77**, N2.— P. 299.
19. Bromberg A.V., Luk'yanovich V.M., Nemtsova V.V. et al. // *Ibid.*— **80**, N 4.— P. 615—617.
20. Beresteneva Z.Ya., Kargin V.A. // *Uspekhi Khim.*— 1955.— **24**, N 3.— P. 249—259.
21. Martinov M.A., Vyglezhanina K.A. *X-Ray Diffractometry of Polymers.*— Moscow: Khimiya, 1972 (in Russian).
22. Wu C.-G., Lin Y.-G., Hsu S.-S. // *Synthetic Metals.*— 1999.— **102**.— P. 1268—1269.
23. Ushakov S.N. *Polyvinyl Alcohol and Its Derivatives.* — Moscow: Izd. AN SSSR, 1960 (in Russian).
24. Sheludko A. *Colloid Chemistry.*— Moscow: Mir, 1984. (in Russian).
25. Bullo J., Cordier P., Gallais O. et al. // *J. Non-Cryst. Solids.* — 1984.— **68**, N1.— P. 135—146.
26. Gharbi N., Sanchez C., Livage J. et al. // *Inorg. Chem.*— 1982.— **21**, N 7.— P. 2758—2765.
27. Volkov V.L., Zakharova G.S., Bondarenka V.M. *Xerogels of Simple and Complicated Polyvanadates.* — Ekaterinburg: Ural Branch of RAS, 2001 (in Russian).
28. Hvilsted S., Andruzzi F., Kulinna C. et al. // *Macromolecules.*— 1995.— **28**.— P. 2172—2183.
29. Nosov Yu.R. *Optoelectronics.*— Moscow: Radio i Svyaz, 1989 (in Russian).
30. Guang S. He, Wung C.J., Xu G.C., Prasad P.N. // *Appl. Opt.*— 1991. — **30**, N27.— P. 3810—3817.

ФІЗИКО-ХІМІЧНІ ТА НЕЛІНІЙНООПТИЧНІ  
ВЛАСТИВОСТІ КВАНТОВИХ ТОЧОК  
ТА КВАНТОВИХ ГОЛОК V<sub>2</sub>O<sub>5</sub> В ПВС

А.С. Куценко, С.М. Малолетов, С.Я. Кучмій,  
В.Р. Ляховецький, В.І. Волков, А.О. Борщ,  
П.М. Литвин

Резюме

Синтезовано новий наноккомпозит V<sub>2</sub>O<sub>5</sub>/ПВС та одержано з нього тонкі плівки, які було досліджено методами електронної (ультрафіолетова, видима та близька інфрачервона спектральні області) та ЕПР-спектроскопії. Присутність квантових точок та квантових голок V<sub>2</sub>O<sub>5</sub> у композиті виявляли за допомогою рентгенівської дифракції та атомного силового мікроскопа. Нелінійність рефракції в наших зразках досліджували у схемі виродженої чотирихвильової взаємодії та Z-сканування. Визначено знак та значення коефіцієнта нелінійності показника заломлення  $n_2$ . Розглядаються можливі механізми нелінійнооптичного відгуку.